ARTICLES
PUBLISHED ONLINE: 14 JUNE 2009 | DOI: 10.1038/NPHYS1306
nature physics

Directing cell motions on micropatterned ratchets

Goher Mahmud, Christopher J. Campbell, Kyle J. M. Bishop, Yulia A. Komarova, Oleg Chaga, Siowling Soh, Sabil Huda, Kristiana Kandere-Grzybowska* and Bartosz A. Grzybowski*

Cell motility is a process deriving from the synchronized dynamics of the cytoskeleton. In several important physiological processes—notably, cancer metastasis—the randomly moving cells can acquire a directional motility phenotype and bias their motions in response to environmental cues. Despite intense research, however, the current understanding of directional cell migration is incomplete and there is a growing need to develop systems that would enable the study and control of this process. This article demonstrates that random motions of motile cells can be rectified by asymmetric ('ratchet') microgeometries. Interactions between the cells and the imposed geometrical cues guide cell polarization and give rise to directional motility. Depending on the ratchet design, cells of different types can move either in the same or in opposite directions on the same imposed pattern. In the latter case, it is possible to partially sort mixed cell populations into different collecting reservoirs.

In the presence of asymmetric potentials generated by time-dependent external fields[1–5] or by asymmetric geometrical obstacles[6–10], objects agitated by random noise can move directionally. This so-called ratcheting phenomenon[11–13] has attracted considerable scientific attention and has been studied extensively in quantum[5], (bio)molecular[14], nanoscopic[7,15] and colloidal[4,8] regimes—albeit, with relatively simple entities (such as electrons[3], small molecules[16], proteins[17], biopolymers[9,14] and microparticles[10]). Here, we show that far more complex and autonomous random movers[18,19]—specifically, motile cells—can also bias their motions over large distances through their interactions with asymmetric geometrical cues. When confined to ratchet-shaped micropatterns, the cells reconfigure their internal motility machinery and undergo sequences of morphological changes that ultimately translate into biased/directional cell motion. Fluorescent imaging suggests that this breaking of spatial symmetry is due to the reorganization of actin bundles, which, in turn, determines the direction of a cell's lamellipodial protrusion[20,21] and cell polarization[22,23]. Biased cell motion can be rationalized by energetic considerations, and the degree of observed directional preference can be modelled by probabilistic methods. The phenomenon of cell ratcheting applies to different cell types and to mixed cell populations. Remarkably, in the latter case, ratchet geometries can be designed that cause cells of different types to migrate in opposite directions. This capability derives from the differences in the morphologies of cell protrusions and provides a basis for microsystems that can partially sort mixed cell populations (here, cancerous versus non-cancerous cells) into spatially disjoint microreservoirs. The microratchets described in this work provide a conceptual alternative to cell guidance using chemical gradients[24–28], which degrade over time and are based on cell-specific chemoattractants (unknown for most cell types). In contrast, microratchets preserve their function unless mechanically broken and can guide cells of different types.

Unidirectional ratchets

Tracks for cell locomotion were microetched in glass/Ti/Au substrates[29,30] and the unetched portions of gold were protected with oligo(ethylene glycol) alkane thiols known to resist cell adhesion[31–34] (Fig. 1a and see the Methods section). When the cells were cultured onto the micropatterned substrates, they localized exclusively onto the etched, unprotected regions. If these regions were bounded in all directions and separated (for example, the equilateral triangular islands shown in Fig. 1b, top), the cells spread on them but did not move. The cells also remained stationary on more elongated triangles such as those used by Whitesides and co-workers[35]. If the regions were bound along only one direction, (that is, straight lines, Fig. 1b, middle), the cells moved randomly in both directions but with no net bias. To guide cell motions, the tracks had to be connected and have asymmetric, ratchet-like geometries distinguishing between the two possible directions of motion.

Figures 1b (bottom) and 2 show one such geometry inspired by well-known fluidic rectifiers[36]. Here, $M = 5$ etched triangles are connected by narrow openings, and either B16F1, Rat2 or MDA-MB-231 cells (initially randomly distributed) move preferentially in the 'funnelling' direction of the patterned triangles—that is, in the direction of a unit triangle's vertex with an opening to the next triangle (henceforth, 'bias direction'). To analyse the degree of this preference and its relation to various system parameters, we quantified it in two ways: (1) on the ratchets, by tracking multiple (>14) cells for extended periods of time (typically, 16 h in 1 h intervals; >220 data points; Table 1 and Supplementary Section S1c) and calculating the percentage of 'steps' these cells took in the bias direction, $b_1 = (n_{\mathrm{bias}}^{\mathrm{rachet}}/n_{\mathrm{total}}^{\mathrm{rachet}}) \cdot 100\%$ and (2) in the reservoirs at the ends of the ratchets (from counts of fixed cells; see Fig. 2a), as the percentage of cells accumulated in the reservoir along the bias direction, $b_2 = (N_{\mathrm{bias}}^{\mathrm{reservoir}}/N_{\mathrm{total}}^{\mathrm{reservoir}}) \cdot 100\%$ at a given time. The first of these measures provided information about short-range bias; the second determined the ratchet's ability to guide cells over longer distances (0.3–1 mm). The optimized values of both b_1 and b_2 for various cell types are summarized in Table 1. In the following, we first discuss the nature of the intracellular processes that give rise to the asymmetry of motion (that is, b_1, $b_2 > 50\%$) and then focus on the parameters (system's geometry, dimensions and so on) affecting the b_1 and b_2 biases.

The origin of asymmetric cell motions

The changes in the cells' cytoskeleton during cell migration on the ratchets were studied in a series of microscopy experiments.

Department of Chemical and Biological Engineering and Department of Chemistry, Northwestern University, 2145 Sheridan Rd, Illinois 60208, USA.
*e-mail: grzybor@northwestern.edu; kanderek@northwestern.edu.

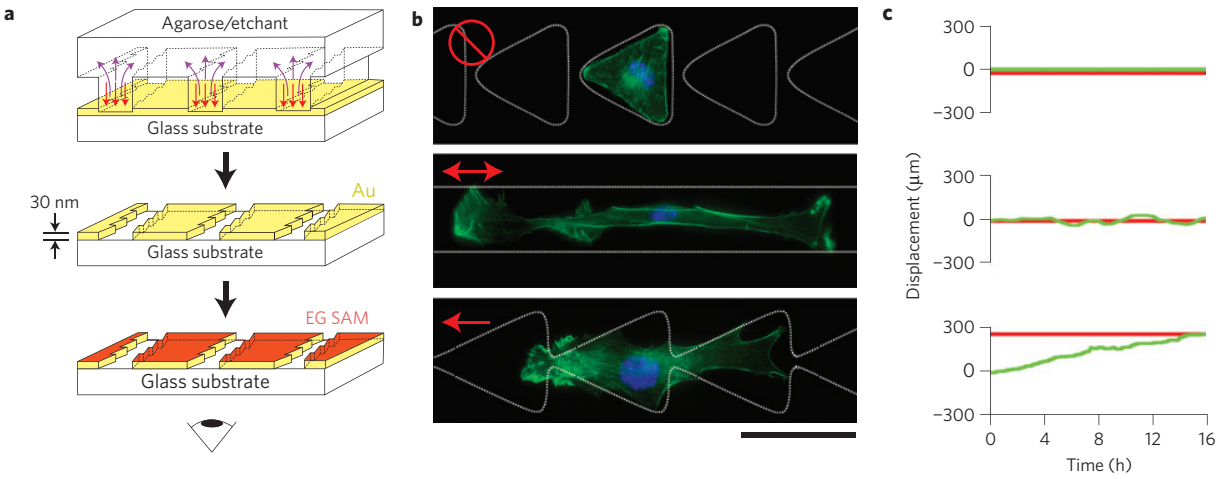

Figure 1 | Fabrication of substrates for cell locomotion and motility characteristics of cells on various micropatterns. a, Anisotropic solid microetching for cell micropatterning uses a micropatterned agarose stamp soaked in TFA Transene etchant to remove the patterned portions of a thin gold film. Once in contact with the substrate, the stamp acts as a two-way diffusive pump constantly delivering the etchant to the gel–substrate interface (orange arrows), while removing the etching products into its own bulk (violet arrows). As etching does not require pre-masking of the unpatterned surface, gold surrounding the transparent areas can be subsequently derivatized with a high-quality, cell-resistant self-assembled monolayer (here, $(HS\text{-}(CH_2)_{11}\text{-}(OCH_2CH_2)_6\text{-}OH$, ProChimia); EG SAM). The 'eye' indicates the position of the objective/imaging direction from below the pattern and through the flat cell–glass interface. **b**, Cells on disconnected triangles do not move (also see Supplementary Section S2a); cells on straight lines move randomly in both directions; cells on triangular ratchets move directionally. The white dotted lines delineate boundaries of the micropatterns. All images show B16F1 cells. Colour coding: actin (green) is stained with fluorescent phalloidin, DNA (blue) is stained with Hoechst 33342 dye. The scale bar corresponds to 50 μm. **c**, The green lines give trajectories of typical cells on the patterns shown in **b**. The red lines correspond to net cell displacement after 16 h.

Table 1 | Statistics of the motility of cells on different types of pattern.

Pattern	Direction of migration	Cell type/substrate*; serum conc. (%)		Bias b_1 from ratchets†	Bias b_2 from reservoirs‡
———	⟷	B16/Fn§	2	50.6% ($n=14/m=224$)	49.7% ($N_T=2{,}047, R=9, Z=0.43$)
▶▶▶	⊘	B16/Fn§	2	No cell motion	No cell motion
▶▶▶	→	B16/Fn	0.5	59.0% ($n=38/m=608$)	65.1% ($N_T=1{,}250, R=32, Z=10.40$)
			2	54.6% ($n=17/m=272$)	60.9% ($N_T=10{,}857, R=32, Z=21.04$)
			10	56.1% ($n=20/m=320$)	55.4% ($N_T=39{,}828, R=96, Z=20.37$)
		Rat2/Ln	2	61.0% ($n=16/m=256$)	60.6% ($N_T=2{,}699, R=13, Z=10.61$)
			10	68.0% ($n=25/m=400$)	61.8% ($N_T=1{,}122, R=45, Z=3.23$)
		MDA-MB-231/Ln	10	57.3% ($n=22/m=352$)	59.7% ($N_T=1{,}420, R=21, Z=7.31$)
◢◣	→	B16/Ln	10	54.9% ($n=14/m=224$)	54.8% ($N_T=11{,}460, R=61, Z=10.2$)
	←	Rat2/Ln	10	62.8% ($n=15/m=240$)	55.8% ($N_T=5{,}874, R=29, Z=8.59$)
	→	MDA-MB-231/Ln	10	58.2% ($n=14/m=224$)	56.3% ($N_T=934, R=11, Z=3.85$)

Straight lines (no bias), disjoint islands (no cell motion) and two types of ratchet (biased motion). All ratchets had $M=5$ unit cells, each of area $a\sim1{,}300\,\mu m^2$.

*Fn: fibronectin; Ln: laminin.

†The biases b_1 were based on live cell imaging. The typical standard deviations in b_1 were of the order of 1–3%. The values of n/m give the total number of analysed cells and data points (16 one-hour intervals per cell).

‡Reservoir biases b_2 were calculated from the counts of cells fixed with formaldehyde in the reservoirs after 48 h. N_T is the total number of cells analysed over R reservoir arrays (~5 ratchet systems per one coverslip used). The values of $Z=(b_2-0.5)/\sqrt{0.25/N_T}=(2b_2-1)\sqrt{N_T}$ are the Z scores of the so-called p test. To determine the validity of the hypothesis (with 99% confidence) that the bias on straight lines is statistically equivalent to 50%, Z must be less than 2.576. For the ratchets, verification of the hypothesis that the bias is statistically greater than 50% requires $Z>2.576$.

§These indicate that qualitatively similar results (that is, no bias on lines and no motion on disjoint islands) were also observed for the Rat2 and MDA-MB-231 cells. We note that no statistically significant reservoir biases were observed immediately after cell plating, $t=0$. This was confirmed by the statistics taken over $R=31$ reservoir arrays and $N_T=7{,}727$ cells, for which the average value of b_2 was 49.5% with $Z=-0.88$ not significantly different from 50% or no bias (also see Supplementary Section S3).

Figure 2b–d (also see Supplementary Video S1') illustrate a typical sequence underlying the guided motion of a B16F1 cell starting from one of the ratchet's triangles. Initially, the cell conforms to the shape of this triangle. Subsequently, it forms a large lamellipodial protrusion into the next triangle and polarizes (as demonstrated by the distribution of Arp2/3 polarity markers) in the direction of the bias. The lamellipodium 'funnels' into the next triangle where it spreads both forward and sideways to 'anchor' against the back-side and corners of the forward triangle (indicated by asterisks in Fig. 2b; also see the focal adhesions in Fig. 3b and Supplementary Video S2). Although lamellipodial extension in the 'backward' direction is sometimes also observed, it is less persistent and cannot 'anchor' against the smooth, 'funnelling' sides of the back triangle (indicated by arrows in Fig. 2b). Overall, the protrusion in the direction of the

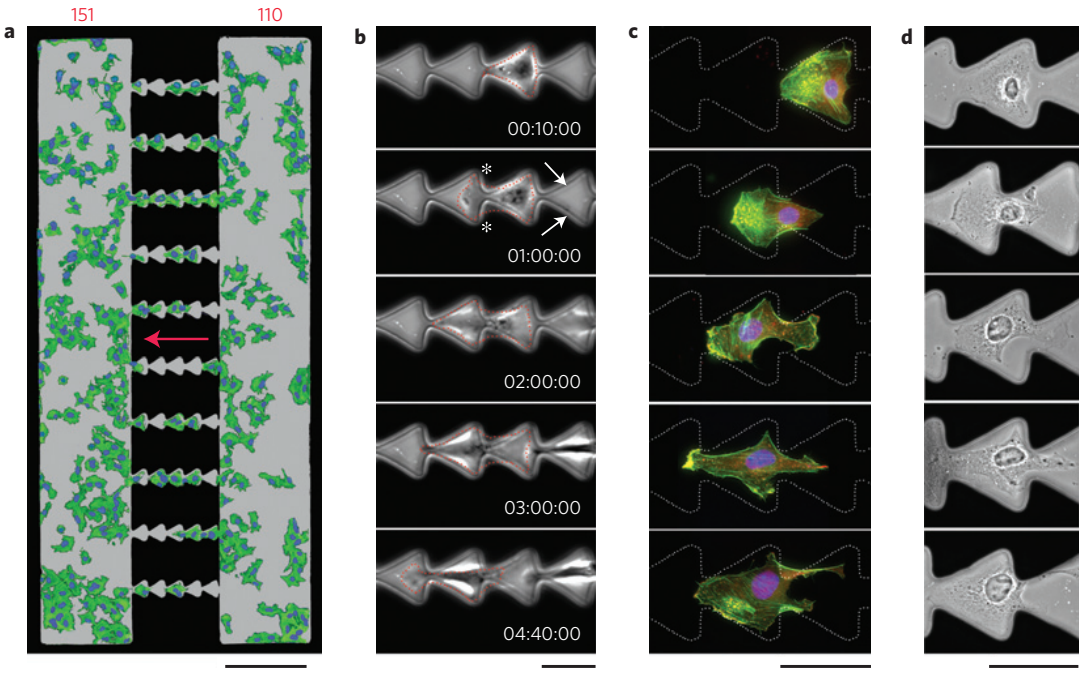

Figure 2 | Directional cell migration on connected-triangle ratchets. a, Distribution of B16F1 cells on a pattern of two reservoirs connected by ten ratchets at 48 h after cell plating (serum concentration 2%). The 57.8% bias illustrated here corresponds to 151 cells collected in the left reservoir and 110 cells in the right one. The red arrow indicates the bias direction. Colour coding: array, grey; actin, fluorescent phalloidin, green; DNA, Hoechst 33342, blue. The scale bar represents 250 μm. **b**, Low-magnification, phase-contrast live images of a B16F1 cell migrating on a ratchet. Live cell imaging were acquired every 10 min. The red dotted lines outline the cell edge. The patterned geometry constrains the cell shape and determines the cell polarity. The cell migrates by repeating a cycle of protrusion (at the cell's leading edge, in the 'funnelling direction') and retraction (at its rear). At ~10 min after plating, the cell adopts a triangular shape, extends a protrusion into the nearest triangle (~1 h), stretches over two triangles (~2 h), moves its nucleus over the narrow opening between triangles (~3 h) and finally contracts its rear while extending a protrusion into the next triangle (~4 h 40 min). The scale bar represents 50 μm. **c**, Distribution of polarity markers (Arp2/3 complex, seen as yellow on overlay images with actin) and organization of actin cytoskeleton (fluorescent phalloidin, green) in cells fixed on the ratchets. The images correspond to different stages of cell migration shown in **b**. The Arp2/3 complex localizes preferentially at the cell's front (that is, in the bias direction). Most pronounced actin stress fibres are along the cell's sides (to constrain the shape of the migrating cell) and at its rear (to help retract its tail). Enhanced accumulation of actin in a lamellipodium at the cell's front reveals actin polymerization into a network of branched actin filaments pushing the membrane forward. The scale bar represents 50 μm. **d**, Phase-contrast images corresponding to those in **c**. The scale bar represents 50 μm.

bias wins this 'tug-of-war', and the cell propels itself along the bias while retracting its tail.

The preferential formation of a lamellipodium in the bias direction reflects an asymmetric distribution of actin and focal adhesions in a cell subject to the ratchet's geometry. This is illustrated in Fig. 3a, b, which shows pronounced actin bundles running along the edges of a unit triangle and 'connecting' the points of highest curvature (that is, spiked edges where most focal adhesions form[30,34]). If the triangle were isolated, these bundles would 'converge' at all three of the triangle's vertices (see Fig. 1a and Supplementary Section S2a). On the ratchets, however, the corner funnelling into to the next triangle is 'open' and the 'side' bundles (indicated by the letter 's' in Fig. 3a) do not converge/connect, leaving between them space through which a lamellipodium can form without disrupting the bundles. In sharp contrast, the bundle at the 'back' of the triangle runs perpendicular (denoted 'p' in Fig. 3a) to the ratchet's axis of symmetry, and if the lamellipodium were to form into the 'back' triangle, this bundle would first have to be disrupted/broken at an energetic cost that can be roughly estimated[37] to be $\sim 5 \times 10^{-18}$ J (from the known energy needed to break one actin filament, 2.38×10^{-19} J, multiplied by the ~20 filaments in one stress bundle). Therefore, it is easier for the cell to make a lamellipodium along the direction of bias than against it. Once the lamellipodium forms and focal adhesions attach to the substrate, the cell's stress fibres reorganize (see Supplementary Section S5).

Analysis of intracellular forces (by high-resolution velocity mapping of the actin stress fibre crosslinker, α-actinin[38]) in a cell trying to enter a new triangle reveals (Fig. 3c, d) that these contractile elements straighten up and align, and that the net force acting on them is directed in the bias direction. At the same time, the forces acting on the cell's rear cause this part of the cell to retract.

Although this explanation of ratcheting is certainly oversimplified in terms of the energetics involved, it can account—at least qualitatively—for the origin of the asymmetry underlying cell ratcheting. Also, a similar sequence of events is observed for MDA-MB-231 and Rat2 cells. We note, however, that the Rat2 cells are more elongated than either B16F1 cells or MDA-MB-231 cells, and in addition to broad lamellipodia, they often form elongated 'exploratory' protrusions extending over more than one triangle ahead of the cell's body (see Supplementary Video S3).

Design and theoretical considerations

The design of efficient ratchets requires understanding and optimization of several parameters of the system (see Supplementary Section S7).

(1) The 'local' bias b_1 reflecting the asymmetry of cell motion depends predominantly on the dimensions of the individual, unit triangles. The largest biases are observed when the area of the unit cell, a, is commensurate with the area of a cell spread on an unpatterned surface (here, $a \sim 1{,}300\,\mu m^2$). On larger triangles, cells cannot interact simultaneously with all imposed

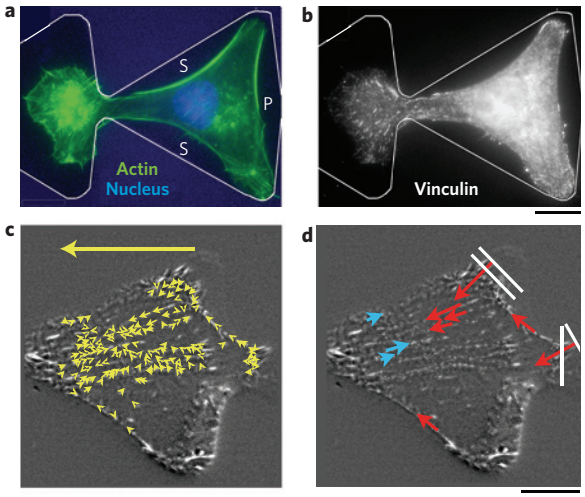

Figure 3 | Mechanism of directional cell migration on micropatterned ratchets. a,**b**, Distribution of actin (**a**) and distribution of focal adhesions (**b**) in a B16F1 cell on a connected-triangle ratchet. Colour coding: array, dark blue; actin, phalloidin, green; DNA, Hoechst 33342, light blue; 's' and 'p' indicate, respectively, the side and the perpendicular actin bundles. The scale bar is the same for **a** and **b** and corresponds to 12.5 μm. **c**,**d**, Analysis of intracellular forces based on live cell imaging of B16F1 cells transiently expressing α-actinin tagged with enhanced green fluorescent protein. **c**, High-resolution velocity map of the displacements of α-actinin markers over a 16.5 min interval. The projections of these displacements onto the ratchet's axis of symmetry sum up to a net displacement of 24.9 μm (large yellow arrow) proportional to the net force (see ref. 38) generated by the actin cytoskeleton in the bias direction. **d**, The map of effective forces acting in the direction of the cell retraction (large red arrows; in regions where the cell contracts) and along the stress fibres (small red arrows are forces acting in the direction of cell migration; blue—in the opposite direction). The white lines give the positions of the retracting parts at 0 and 19 min. The scale bar is the same for **c** and **d** and corresponds to 12.5 μm.

boundaries, and move within the triangles with less overall bias (no statistically significant bias for $a > \sim 1{,}800\,\mu m^2$). For smaller values of a, the cells are spread over several triangles and even some oligo(ethylene glycol) self-assembled monolayer areas, and also move less directionally (no bias for $a < \sim 1{,}000\,\mu m^2$). Furthermore, the biases are maximal when the width of the opening connecting the triangles is ~10–20 μm. For smaller openings, the cells cannot squeeze efficiently through narrow 'funnels' and move only sporadically (once every few hours); for larger ones, they can travel more freely along either of the two possible directions (with no net bias for opening width > ~30 μm).

(2) Bias b_2 responsible for the guidance over larger distances depends not only on the local bias but also on the number of the unit triangles in the ratchet and the dimensions of the cell reservoirs. We first estimate the probability that a cell that has already entered a ratchet channel from one reservoir, will pass all the way through this channel into the other reservoir. We approximate the cell as a random walker on a one-dimensional lattice with periodicity Δx determined from experimental ratchet dimensions (here, $\Delta x \sim 54\,\mu m$) and time steps, calculated from experimental velocities, v, of cells on ratchets (for example, for B16F1 cells under 2% serum conditions, $v \sim 30\,\mu m\,h^{-1}$ and $\Delta t = \Delta x/v = 42.5\,\mu m/24\,\mu m\,h^{-1} = 1.8\,h$). The probability p_l of a cell taking a step in the direction of the bias ('to the left' in Fig. 4a) is given by the experimentally determined value of b_1 (for example, 54.6% for B16F1 in 2% serum, see Table 1); the probability of the cell taking a step against the bias, 'to the right' is $p_r = 1 - p_l$. With these considerations, one may calculate the probabilities[39] that after time $t = n\Delta t$, the cell will have successfully crossed the channel from right to left, $P_L(n)$:

$$\begin{aligned} P_L(n) = & \sum_j \left\{ p_l^{M(j+1)-x_0} p_r^{Mj} \sum_i \binom{n}{i} (p_l^{n-M(1+2j)+x_0-i} p_r^i \right. \\ & \left. + p_r^{n-M(1+2j)+x_0-i} p_l^i) \right\} \\ & - \sum_j \left\{ p_l^{M(j+1)} p_r^{Mj+x_0} \sum_i \binom{n}{i} (p_l^{n-M(1+2j)-x_0-i} p_r^i \right. \\ & \left. + p_r^{n-M(1+2j)-x_0-i} p_l^i) \right\} \end{aligned} \quad (1)$$

In this equation, M is the number of ratchet units (here, the triangles) along the channel and x_0 is the initial position of the cell walker (here, always taken as $x_0 = 1$—that is, cells start in the first ratchet). The summation over $i \geq 0$ continues until the terms in the series in each curly bracket, rearranged in descending powers of p_l, meet in the middle (the middle term counting only once if $n - M + x_0$ is even, see Supplementary Section S6.1); the summation over t covers all values $j \geq 0$ that leave non-negative exponents. An expression for the crossing from the 'left to the right', $P_R(n)$, may be obtained from the above expression by exchanging p_l and p_r. For large n (corresponding to long times, $t = n\Delta t$), $P_L(n)$ and $P_R(n)$ converge to the following asymptotic values:

$$\begin{aligned} P_L &= [(p_r/p_l)^{x_0} - 1]/[(p_r/p_l)^M - 1] \quad \text{and} \\ P_R &= [(p_l/p_r)^{x_0} - 1]/[(p_l/p_r)^M - 1] \end{aligned} \quad (2)$$

Figure 4b illustrates the case in which $p_l = 0.546$ (in experiments, B16F1 in 2% serum) and $M = 5$, for which the asymptotic probability of crossing the channel from right to left is 0.28 (the crossing is unsuccessful with probability 0.72). Note that the case of cells entering the ratchet from the 'left' and migrating against the bias towards the 'right' reservoir is solved analogously (for the particular cell type discussed above, the cell has a 13% chance of making it all the way through against the bias).

Using the rate of cells entering the channels (~5 cells h^{-1}; see the Methods section) and the probability of passing through the channel (equations (1) and (2)), it is possible to relate the b_1 and b_2 biases and describe how the numbers of cells in the reservoirs change in time. Let N_L and N_R denote the number of cells in the 'left' and 'right' reservoirs, respectively. The population balances for the number of cells in reservoirs L and R are expressed as

$$\frac{dN_L}{dt} = k_L \frac{N_R}{1 - \alpha N_R} - k_R \frac{N_L}{1 - \alpha N_R} + k_g N_L (1 - \alpha N_L) \quad (3)$$

$$\frac{dN_R}{dt} = k_R \frac{N_L}{1 - \alpha N_L} - k_L \frac{N_R}{1 - \alpha N_R} + k_g N_R (1 - \alpha N_R) \quad (4)$$

Here, $\alpha = a/A$, $k_L = CL_c VP_L/2A$ and $k_R = CL_c VP_R/2A$, parameters C, L_c, V and A are defined in the Methods section and P_L and P_R are the probabilities of a cell passing though the channels from right to left (R → L) and from left to right (L → R), respectively (see above). The last terms in the above equations describe the logistic growth of the cell populations (see Supplementary Section S6.2) with a growth rate, $k_g \sim 0.035\,h^{-1}$ (that is, doubling time of 20 h, as in the experiments) and a carrying capacity of $1/\alpha \sim 250$ (that is, 250 cells of area $a \sim 1{,}300\,\mu m^2$ cover the full area A of each reservoir). The set of nonlinear differential equations equations (3) and (4) can

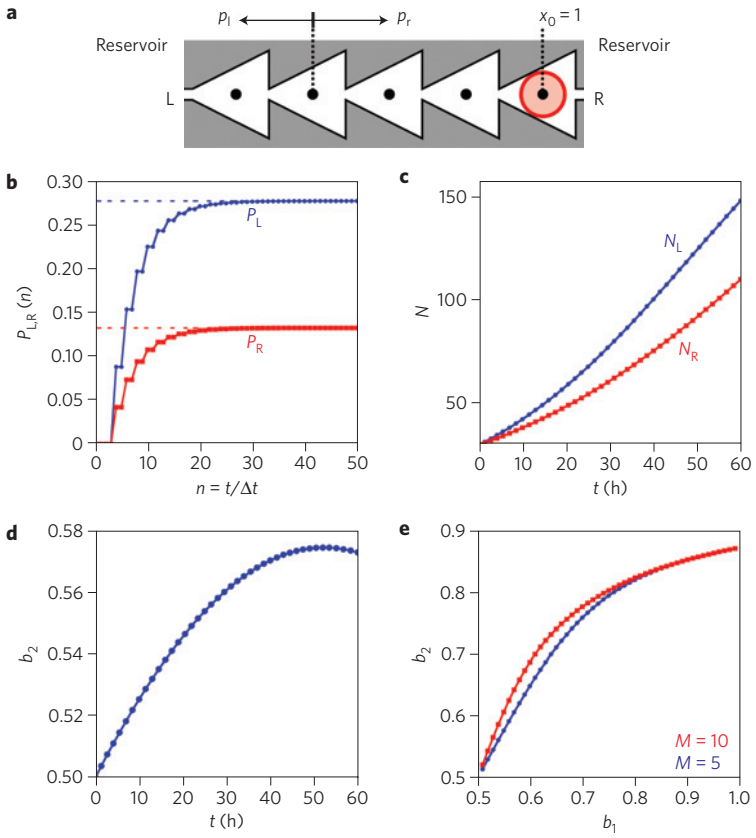

Figure 4 | Probabilities of directional migration, ratcheting efficiency and the scaling properties of the reservoir bias, b_2. a, Schematic illustration of the model geometry. A cell (red), initially located at $x_0 = 1$, moves across the ratcheted channel from reservoir R to reservoir L with probability P_L, which depends on the single-ratchet probabilities, p_l and p_r, for stepping left and right, respectively. **b**, Probabilities of crossing a channel of $M = 5$ ratchets in the bias direction, P_L, and against the bias direction, P_R, as a function of the number of steps n taken. Here, the underlying single-ratchet stepping probabilities are $p_l = 0.546$ and $p_r = 0.454$ corresponding to the experiment with B16F1 cells in 2% serum. **c**, Cell populations, N, in reservoirs L and R as a function of time for the experimental/model parameters presented in the text ($V = 60\,\mu m\,h^{-1}$, $a = 1{,}300\,\mu m^2$, $A = 320{,}000\,\mu m^2$, $CL_c = 10 \times 35\,\mu m$, $P_L = 0.28$ and $P_R = 0.13$). **d**, The b_2 reservoir bias for data in **c** as a function of time. The maximum bias is achieved after ~48 h, after which cell division/growth begins to overcome the effect of the ratchets. **e**, The b_2 reservoir bias as a function of the underlying b_1 ratchet bias for $M = 5$ and $M = 10$ ratchets and for 48 h of ratcheting.

be solved numerically. For example, for the typical experimental conditions for B16F1 cells in 2% serum described here, the crossing rates are estimated as $k_L = 0.0092\,h^{-1}$ and $k_R = 0.0043\,h^{-1}$ to give the time-dependent cell populations in the reservoirs (Fig. 4c). These values allow for the calculation of the time dependence of bias $b_2 = N_L/(N_R + N_L)$ (Fig. 4d), of which the final value at ~50 h is ~57.7%—that is, close to 60.9% observed experimentally for B16F1 cells in 2% serum (see Table 1). Similar agreement is observed for other conditions and cell types. In addition, as illustrated in Fig. 4e for $M = 5$ and $M = 10$, the values of b_2 increase only slowly with increasing number of unit triangles in the ratchet channel. Again, this observation is in agreement with experiments and reflects the fact that making ratchets longer significantly decreases the probability of cells crossing in either direction—in other words, P_L and P_R decrease significantly despite the fact that the ratio P_L/P_R increases. Finally, the model correctly predicts that for times longer than ~50 h, the growth of the cells will take over the ratcheting, until both reservoirs are fully populated with no bias. Therefore, 48 h used in experiments is close to the 'optimal' time for ratchet operation (see Supplementary Section S3 for time analysis).

Two-directional ratchets

The applicability of the one-directional ratchets discussed so far is probably limited to the mechanistic studies of cell migration in well-defined microgeometries. Ratchets that could guide cells of different types in opposite directions would be much more useful, especially in the context of cell sorting[40–42] and related medical diagnostics[43,44]. We investigated the possibility of such two-directional ratchets based on the differences in the morphology of cells' protrusions—for instance, the broad lamellipodia formed by the cancerous B16F1 or MDA-MB-231 cells and the combination of lamellipodia and long, 'exploratory' protrusions of non-cancerous Rat2 fibroblasts (see Supplementary Video S3). As mentioned before, the long protrusion of the Rat2 cell extends more than one triangle ahead of the cell's body and often 'anchors' against the 'obstacles' (for example, the sides of the ratchet's triangles) within the confining channels. Although for triangular ratchets this phenomenon has negligible effect on the overall direction of motion, it could be made more manifest if the in-channel protrusions were more pronounced.

This reasoning guided the design of morphology-based ratchets on which B16F1 and Rat2 (or MDA-MB-231 and Rat2) cells move in opposite directions. In these ratchets, the asymmetric 'spike' protrusions alternate on the opposite sides of the channel (Fig. 5a). If the cells are compact (Fig. 5a, left), they spread on the ratchet, contact the boundaries on the opposite walls and therefore experience a 'funnel'-like geometry akin to that in the one-directional ratchets. Both live imaging as well as immunostaining experiments showed that B16F1 cells and MDA-MB-231 behave in this way and form lamellipodia that are broader near the short base of a unit trapezium than near the 'open' vertex of a long base (see Fig. 5a, left). Consequently, these cells polarize towards

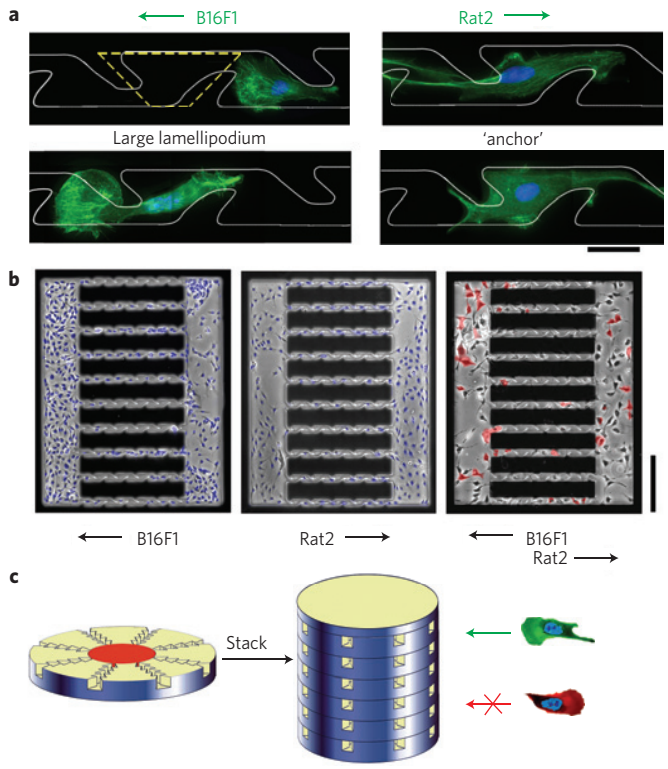

Figure 5 | Cells on bi-directional 'lines-with-spikes' ratchets. a, B16F1 and Rat2 cells move in opposite directions on linear ratchets with spikes inclined at 45° (staining: phalloidin, green; Hoechst 33342, blue). B16F1 cells (left column) form large lamellipodial protrusions near the 'open' vertices of the short base of a unit trapezium (delineated by a yellow dotted line, adhesive area ~1,300 μm^2). In contrast, Rat2 cells extend long protrusions into the 'open' vertex of a long base (top) and 'anchor' at the nearby spike. The borders between adhesive and non-adhesive areas are outlined by dotted lines. The scale bar corresponds to 30 μm. **b**, Distribution of B16F1 (left), Rat2 (middle) and a mixture of B16F1 and Rat2 (right) cells over a pattern of two reservoirs connected by ten spiked ratchets (after 48 h from cell plating, also see Supplementary Section S3; serum concentration 10%; laminin). Superimposed images of phase contrast and nuclei (Hoechst 33342, blue) illustrate 54.8% bias for B16F1 cells (189 cells in the left reservoir and 156 in the right one) and 56.0% bias for Rat2 (80 and 102 cells). For the mixture of B16F1 cells and Rat2 cells, the former are stained with a red DiI dye; the image is a superposition of phase contrast and DiI. The cells of two types partly sort out and the biases from reservoir counts are 57.7% bias for B16F1 cells (15 cells in the left reservoir and 11 in the right one) and 56.5% bias for Rat2 cells (27 and 35 cells). The scale bar represents 250 μm. **c**, An idea for a 'cancer trap' comprising stacks of radially arranged ratchet channels. When implanted next to a tumour, the channels could selectively guide motile cancerous cells (green) inwards, but not other cells (red).

this large lamellipodium, which then spreads into the next unit cell and facilitates the overall migration of the cell with biases $b_1 = 54.9\%$; $b_2 = 54.8\%$ for B16F1 and $b_1 = 58.2\%$; $b_2 = 56.3\%$ for MDA-MB-231 cells (Table 1). In sharp contrast, the elongated Rat2 cells do not contact all ratchet boundaries but instead use their long protrusions to 'grab' against the in-channel spikes, preferentially around the spikes slanted in the protrusion's direction (that is, to the right in Fig. 5a, also see Supplementary Video S4). Once an 'anchor' is stabilized by focal adhesions, the protrusion lays down a larger lamellipodium around it, and the cell pulls the trailing part of its body into the new location. The on-ratchet biases for the Rat2 cells were $b_1 = 62.8\%$ and $b_2 = 55.8\%$.

Importantly, the biased motions were also observed on ratchets plated simultaneously with two cell types (specifically, B16F1/Rat2 or MDA-MB-231/Rat2 pairs; Fig. 5b, rightmost image). Starting from an initial, uniform distribution over the pattern, the ratchets moved cells of different types in opposite directions—B16F1 cells or MDA-MB-231 along the 'funnels' and Rat2 cells along the slant of the spiked in-channel obstacles. The morphological and structural changes accompanying these migrations were similar to those observed in the single-cell-type experiments described in the previous paragraph. Although the b_1 biases on the ratchets could not be directly assigned (as live imaging of cells labelled with fluorescent dyes caused photo-damage and reduced their motility), the counts over the reservoirs after 48 h showed that the cells partly sorted out. For the B16F1/Rat2 pair, the biases were b_2 (B16F1) = 55.0% and b_2 (Rat2) = 56.3% (data based on 30 reservoir pairs with a total of 702 B16F1 and 2788 Rat2 cells; Z scores >6 for both cell types). For the MDA-MB-231/Rat2 pair, b_2 (MDA-MB-231) = 57.3% and b_2 (Rat2) = 63.4% (data based on 47 reservoir pairs with a total of 1012 MDA-MB-231 and 3513 Rat2 cells; Z scores > 10 for both cell types). We observe that because these values are close to those from single-cell-type experiments on the same ratchet, it seems that interactions between B16F1 cells and Rat2 cells do not affect the motility of either cell type perceptibly (see Supplementary Section S4c). We also note that control experiments with reservoirs connected by straight lines showed no bias, indicating that directional cell guiding on the spike ratchets is a consequence of the imposed geometry alone.

Outlook

If optimized further to achieve significantly higher biases and longer operational times, ratchet microsystems could find uses in sorting motile cells of different[42,44–48] types. Of course, the design of ratchet systems should not be confined to planar substrates and parallel channels. Concentric arrangements of two-directional ratchets such as the one proposed in Fig. 5c could be considered, whereby only the motile/metastatic cells were drawn towards the centre and permanently trapped therein. Fabrication of such 'cancer traps' and their potential extension to implantable materials could underlie a new approach to cancer therapy—one based on the physical principle of ratcheting. Finally, cell ratchets offer several opportunities for further theoretical research in biophysics where the quantitative relationship(s) between the imposed geometry and the cytoskeletal processes underlying cell motility remains elusive.

Methods

Experimental set-up. Tracks for cell locomotion were microetched in glass/Ti/Au substrates using the so-called anisotropic solid microetching technique[29,30]. Briefly, agarose stamps micropatterned in bas relief were first soaked in a solution of a gold etchant for ~1 min, blotted dry under a stream of nitrogen for ~30 s and applied onto an electron-beam evaporated layer of gold (30 nm Au, 5 nm Ti adhesion layer) to etch the metal at the regions of contact (see Fig. 1a). The remaining portion of the gold film was then covered with a self-assembled monolayer of oligo(ethylene glycol) alkane thiol ($HS–(CH_2)_{11}–(OCH_2CH_2)_6–OH$, ProChimia) known to resist cell adhesion[31–34]. The etched glass/Ti regions were coated with either fibronectin or laminin and the slides were incubated in a 1% BSA solution for 15 min. The substrates thus prepared offered high optical contrast between the cell-adhesive and non-adhesive regions, and facilitated visualization of the boundaries of the imprinted patterns. In addition, the transparency of the adhesive areas allowed for fluorescent imaging inside the adhered, living cells[30]. The motile cells considered in this study were B16F1 mouse melanoma, Rat2 fibroblasts and MDA-MB-231 human breast carcinoma, all plated at a density of 10,000–20,000 cells cm^{-2} (for further experimental details on patterning and cell culturing, see Supplementary Section S1).

Probabilities of cells entering the ratchets from reservoirs. Initially, N cells are distributed randomly over the entire reservoir of area A (typically, ~320,000 μm^2) and move about at random with a characteristic velocity V (for example, $V \sim 60\,\mu m\,h^{-1}$ for B16F1 on planar substrates; note that V is, in general, different to the velocity v on the ratchet). Neglecting the persistence[49] of the cell motions, the rate per unit length at which cells 'collide' with the walls of the reservoir may

be estimated using the formulae from the kinetic theory of gases (specifically, the rate of collisions of randomly moving particles with the walls) and the van der Waals equation of state accounting for the area taken by the cells themselves: $NV/2A_{\mathrm{free}}$, where $A_{\mathrm{free}} = A - Na$ is the 'free' area unoccupied by cells and a is the average area per cell (typically, $a \sim 1{,}300\,\mu\mathrm{m}^2$). Thus, the rate at which cells enter the channel is simply the above relation multiplied by the length of the channel entrance, L_c, and the number of channels, C—that is, the rate of entering the channel is $NCL_cV/2(A-Na)$. For a typical experimental system of $C = 10$ ratchet channels each with $L_c \sim 35\,\mu\mathrm{m}$ entrance (see Fig. 2a), for two reservoirs of typical area $A = 320{,}000\,\mu\mathrm{m}^2$ each, and with ~120 cells evenly distributed on the reservoirs (typical number of cells at the midpoint of the experiment, at 24 h), the total rate at which cells enter the channels is ~5 cells h^{-1}. Thus, over the course of the experiment (48 h), each cell is expected to enter a channel on average twice. From a practical/design point of view, it is important to note that the chances of cells entering the ratchets decrease with increasing reservoir area (for a fixed number of cells).

Received 4 January 2009; accepted 14 May 2009; published online 14 June 2009

References

1. Lee, S. H. & Grier, D. G. One-dimensional optical thermal ratchets. *J. Phys. Condens. Matter* **17**, S3685–S3695 (2005).
2. Lee, C. S., Janko, B., Derenyi, I. & Barabasi, A. L. Reducing vortex density in superconductors using the 'ratchet effect'. *Nature* **400**, 337–340 (1999).
3. Lorke, A. *et al.* Far-infrared and transport properties of antidot arrays with broken symmetry. *Physica B* **251**, 312–316 (1998).
4. Rousselet, J., Salome, L., Ajdari, A. & Prost, J. Directional motion of Brownian particles induced by a periodic asymmetric potential. *Nature* **370**, 446–448 (1994).
5. Engel, A., Muller, H. W., Reimann, P. & Jung, A. Ferrofluids as thermal ratchets. *Phys. Rev. Lett.* **91**, 060602 (2003).
6. Linke, H. *et al.* Experimental tunneling ratchets. *Science* **286**, 2314–2317 (1999).
7. van Oudenaarden, A. & Boxer, S. G. Brownian ratchets: Molecular separations in lipid bilayers supported on patterned arrays. *Science* **285**, 1046–1048 (1999).
8. Villegas, J. E. *et al.* A superconducting reversible rectifier that controls the motion of magnetic flux quanta. *Science* **302**, 1188–1191 (2003).
9. Hiratsuka, Y., Tada, T., Oiwa, K., Kanayama, T. & Uyeda, T. Q. P. Controlling the direction of kinesin-driven microtubule movements along microlithographic tracks. *Biophys. J.* **81**, 1555–1561 (2001).
10. Matthias, S. & Muller, F. Asymmetric pores in a silicon membrane acting as massively parallel Brownian ratchets. *Nature* **424**, 53–57 (2003).
11. Reimann, P. Brownian motors: Noisy transport far from equilibrium. *Phys. Rep.-Rev. Sec. Phys. Lett.* **361**, 57–265 (2002).
12. Astumian, R. D. & Hanggi, P. Brownian motors. *Phys. Today* **55**, 33–39 (2002).
13. Feynman, R. P., Leighton, R. B. & Sands, M. L. *The Feynman Lectures on Physics* Vol. 1 (Pearson/Addison-Wesley, 2006).
14. Peskin, C. S., Odell, G. M. & Oster, G. F. Cellular motions and thermal fluctuations—the Brownian ratchet. *Biophys. J.* **65**, 316–324 (1993).
15. Silva, C. C. D., de Vondel, J. V., Morelle, M. & Moshchalkov, V. V. Controlled multiple reversals of a ratchet effect. *Nature* **440**, 651–654 (2006).
16. Kelly, T. R., De Silva, H. & Silva, R. A. Unidirectional rotary motion in a molecular system. *Nature* **401**, 150–152 (1999).
17. Simon, S. M., Peskin, C. S. & Oster, G. F. What drives the translocation of proteins. *Proc. Natl Acad. Sci. USA* **89**, 3770–3774 (1992).
18. Alt, W. Biased random-walk models for chemotaxis and related diffusion approximations. *J. Math. Biol.* **9**, 147–177 (1980).
19. Dunn, G. A. & Brown, A. F. A unified approach to analyzing cell motility. *J. Cell Sci. Suppl.* **8**, 81–102 (1987).
20. Theriot, J. A. & Mitchison, T. J. Actin microfilament dynamics in locomoting cells. *Nature* **352**, 126–131 (1991).
21. Ponti, A., Machacek, M., Gupton, S. L., Waterman-Storer, C. M. & Danuser, G. Two distinct actin networks drive the protrusion of migrating cells. *Science* **305**, 1782–1786 (2004).
22. Thery, M. *et al.* Anisotropy of cell adhesive microenvironment governs cell internal organization and orientation of polarity. *Proc. Natl Acad. Sci. USA* **103**, 19771–19776 (2006).
23. Thery, M., Pepin, A., Dressaire, E., Chen, Y. & Bornens, M. Cell distribution of stress fibres in response to the geometry of the adhesive environment. *Cell Motil. Cytoskeleton* **63**, 341–355 (2006).
24. Jiang, X. Y. *et al.* A general method for patterning gradients of biomolecules on surfaces using microfluidic networks. *Anal. Chem.* **77**, 2338–2347 (2005).
25. Dertinger, S. K. W., Jiang, X. Y., Li, Z. Y., Murthy, V. N. & Whitesides, G. M. Gradients of substrate-bound laminin orient axonal specification of neurons. *Proc. Natl Acad. Sci. USA* **99**, 12542–12547 (2002).
26. Brandley, B. K. & Schnaar, R. L. Tumor-cell haptotaxis on covalently immobilized linear and exponential gradients of a cell-adhesion peptide. *Dev. Biol.* **135**, 74–86 (1989).
27. Smith, J. T. *et al.* Measurement of cell migration on surface-bound fibronectin gradients. *Langmuir* **20**, 8279–8286 (2004).
28. Plummer, S. T., Wang, Q., Bohn, P. W., Stockton, R. & Schwartz, M. A. Electrochemically derived gradients of the extracellular matrix protein fibronectin on gold. *Langmuir* **19**, 7528–7536 (2003).
29. Campbell, C. J., Smoukov, S. K., Bishop, K. J. M., Baker, E. & Grzybowski, B. A. Direct printing of 3d and curvilinear micrometer-sized architectures into solid substrates with sub-micrometer resolution. *Adv. Mater.* **18**, 2004–2008 (2006).
30. Kandere-Grzybowska, K., Campbell, C., Komarova, Y., Grzybowski, B. A. & Borisy, G. G. Molecular dynamics imaging in micropatterned living cells. *Nature Meth.* **2**, 739–741 (2005).
31. Maroudas, N. G. Polymer exclusion, cell adhesion and membrane-fusion. *Nature* **254**, 695–696 (1975).
32. Prime, K. L. & Whitesides, G. M. Self-assembled organic monolayers—model systems for studying adsorption of proteins at surfaces. *Science* **252**, 1164–1167 (1991).
33. Singhvi, R. *et al.* Engineering cell-shape and function. *Science* **264**, 696–698 (1994).
34. Kandere-Grzybowska, K. *et al.* Cell motility on micropatterned treadmills and tracks. *Soft Matter* **3**, 672–679 (2007).
35. Jiang, X. Y., Bruzewicz, D. A., Wong, A. P., Piel, M. & Whitesides, G. M. Directing cell migration with asymmetric micropatterns. *Proc. Natl Acad. Sci. USA* **102**, 975–978 (2005).
36. Groisman, A. & Quake, S. R. A microfluidic rectifier: Anisotropic flow resistance at low reynolds numbers. *Phys. Rev. Lett.* **92**, 094501 (2004).
37. Grazi, E., Cintio, O. & Trombetta, G. On the mechanics of the actin filament: The linear relationship between stiffness and yield strength allows estimation of the yield strength of thin filament *in vivo*. *J. Muscle Res. Cell Motil.* **25**, 103–105 (2004).
38. Brown, C. M. *et al.* Probing the integrin-actin linkage using high-resolution protein velocity mapping. *J. Cell Sci.* **119**, 5204–5214 (2006).
39. Thatcher, A. R. Studies in the history of probability and statistics vi. A note on the early solutions of the problem of the duration of play. *Biometrika* **44**, 515–518 (1957).
40. Kumar, A., Galaev, I. Y. & Mattiasson, B. (eds) *Cell Separation: Fundamentals, Analytical and Preparative Methods* Vol. 106 (Springer, 2007).
41. Steinberg, M. S. & Takeichi, M. Experimental specification of cell sorting, tissue spreading, and specific spatial patterning by quantitative differences in cadherin expression. *Proc. Natl Acad. Sci. USA* **91**, 206–209 (1994).
42. Xu, Q. L., Mellitzer, G., Robinson, V. & Wilkinson, D. G. *In vivo* cell sorting in complementary segmental domains mediated by eph receptors and ephrins. *Nature* **399**, 267–271 (1999).
43. Keren, D. F., McCoy, J. P. & Carey, J. L. *Flow Cytometry in Clinical Diagnosis* 3rd edn (American Society Clinical Pathology, 2001).
44. Jennings, C. D. & Foon, K. A. Recent advances in flow cytometry: Application to the diagnosis of hematologic malignancy. *Blood* **90**, 2863–2892 (1997).
45. Steinberg, M. S. Reconstruction of tissues by dissociated cells. *Science* **141**, 401–408 (1963).
46. Townes, P. L. & Holtfreter, J. Directed movements and selective adhesion of embryonic amphibian cells. *J. Exp. Zool.* **128**, 53–120 (1955).
47. Discher, D. E., Janmey, P. & Wang, Y. L. Tissue cells feel and respond to the stiffness of their substrate. *Science* **310**, 1139–1143 (2005).
48. Wyckoff, J. B., Segall, J. E. & Condeelis, J. S. The collection of the motile population of cells from a living tumor. *Cancer Res.* **60**, 5401–5404 (2000).
49. Gail, M. H. & Boone, C. W. Locomotion of mouse fibroblasts in tissue culture. *Biophys. J.* **10**, 980–993 (1970).

Acknowledgements

This work was supported by the NCI Northwestern CCNE (NIH 1U54CA119341-01), the Pew Scholars Program in the Biomedical Sciences (to B.A.G.) and the Sloan Fellowship (to B.A.G.). G.M. was supported by a Gates Fellowship. C.J.C. was supported by a Northwestern University Presidential Fellowship. K.J.M.B. was supported by an NSF Graduate Research Fellowship. K.K.-G. was supported by a Fellowship from a Department of Defense Breast Cancer Research Program (W81XW4-05-1-0312).

Author contributions

G.M. C.J.C, Y.A.K. and K.K.-G. carried out most experiments and data analysis; Y.A.K., K.K.-G., O.C. and S.H. carried out high-resolution in-cell imaging; K.J.M.B. and S.S. developed the theoretical model; K.K.-G. and B.A.G. conceived the experiments and wrote the paper.

Additional information

Supplementary information accompanies this paper on www.nature.com/naturephysics. Reprints and permissions information is available online at http://npg.nature.com/reprintsandpermissions. Correspondence and requests for materials should be addressed to K.K.-G. or B.A.G.